Geologica Acta, Vol.7, Nº 3, September 2009, 333-350
DOI: 10.1344/105.000001441
Available online at www.geologica-acta.com

geologica acta

Extensional stresses in the Colombian Eastern Cordillera fold-and-thrust belt (northern Andes): insights from 2D finite element modeling

MD. RAFIQUL ISLAM* and DAIGORO HAYASHI

Simulation Tectonics Laboratory
Faculty of Science, University of the Ryukyus, 903-0213, Okinawa, Japan. E-mail: rafiqbcmp@yahoo.com

*Corresponding author

ABSTRACT

Deformation and stress characteristics in the upper crust of the fold-and-thrust belt in the Colombian Eastern Cordillera were investigated by numerical analysis. The structural trend of Colombian Eastern Cordillera has long been considered a possible example of a true contraction orogen. The issue of the convergent displacement along an elastic structural body, which controls present-day deformation in this Cordillera is examined here. Modeling results are presented in terms of three parameters: 1) distributions, orientations, and magnitudes of principal stresses; 2) maximum shear stress (τ_{max}) contour; and 3) proximity to failure of elements within faults. Mohr-Coulomb failure criteria with bulk rock properties are applied to analyze the faults. The model shows extensional stresses in the crust at shallow crustal levels (from surface to about 6 km) despite overall contraction, and contraction at depth is confirmed. Measurement results indicate that, for homogeneous crustal thickening, extensional stresses are concentrated in the Servita half-gaben and Bucaramanga fault systems, where the vertical thrust faults and thickening processes are located. Our two-dimensional (2D) modeling results emphasize that extensional stresses are still active along the vertical to sub-vertical fault system in the fold-and-thrust belt of the Colombian Eastern Cordillera.

KEYWORDS | **Finite element (FE) modeling. Elastic rock properties. Convergent displacement. Extensional stress field. Colombian Eastern Cordillera.**

INTRODUCTION

Extension of upper crustal rocks within contractional orogenic belts is very common in many tectonically active zones of the Earth (Dewey, 1988; Malavielle, 1993; Crespi et al., 1996). Active extensional deformation in the Himalayas (Hodges et al., 1992), the Taiwan collision zone (Crespi et al., 1996), and the Southern Apennines of Italy (Caiazzo et al., 2006) has been extensively studied over the past 20 years. This type of deformation is also common in some segments of the Andes. The relevance of extensional stresses in the Andes fold-and-thrust belt has been the subject of many studies. For instance, extensional deformation is still active at the upper crustal part of the southernmost tip of the Patagonian Andes (Klepeis and Austin, 1997). In the Western and Northwestern Argentine Cordillera, extensional tectonics and gravitational collapse are recognized by Charrier et al. (2002), Carrera et al. (2006) and Alonso et al. (2008). According to Richardson and Coblentz (1994), high topographic zones,

especially the Cordillera Blanka region of the central Andes, exhibit both compressional and extensional deformation. In the northern Andes, Jurassic rift structures and Neogene inversion structures at the Merida Andes and the eastern Sierra de Perija mountains in Venezuela have been thoroughly studied by Duerto et al. (2006).

Tectonically, the Colombian Eastern Cordillera of the northern Andes has been an active region for millions of years. Along this part of the Andes, about 90 km of crustal shortening occurred between the Colombia-Ecuador trench and the Eastern Cordillera during Cenozoic time (Corredor, 2003a; fig. 3). In the Colombian Andes, extensional deformation in the Mesozoic and Cenozoic times has been studied extensively by Corredor (2003a), and Sarmiento et al. (2006), but the present-day stress state is unknown. Thus, the basic question is whether extensional strain/stress is still active along the thick-skinned crustal portion of the Eastern Cordillera. The problem is still unresolved because it has not yet been quantitatively tested by modeling the dynamic interactions involved in the crustal deformation.

The tectonic characteristics of the area have been studied by many authors, e.g., Pennington (1981); Freymueller et al. (1993); Cooper et al. (1995); Ego et al. (1996); MacDonald et al. (1996); Trenkamp et al. (2002); Corredor (2003a); Corredor (2003b); Vasquez and Altenberger (2005); Montes et al. (2005); Duerto et al. (2006); Molina et al. (2006); Nivia et al. (2006); and others. However, much less attention has been paid to the contemporary stress field of this region. Additionally, there have been no studies in which thick-skinned fold-and-thrust belts were combined and used to explain the present-day state of stress from a geodynamic point of view. The aim of this study is to analyze relationships between tectonics and stress/strain regimes along the thick-skinned crustal portion of the Colombian Eastern Cordillera. We will focus on a well-documented new example of present-day extensional strain in this back-arc area, although the area is located within a contractional orogenic belt of the northern Andes. Our database includes a regional geological cross-section (Corredor, 2003a) and a finite element method (FEM) software package coded by Hayashi (2008).

A BRIEF OUTLINE OF THE FINITE ELEMENT METHOD

The finite element method was originally developed as a concept of structural analysis and, until now, has mainly been applied to civil engineering problems. However, the wide basis of the method also makes it applicable to such diverse problems as those of fluid flow, heat conduction, vibration and stability, ad so on. (Stephanson and Berner, 1972). Nowadays, this method is very popular among structural geologists. In this investigation, the finite element method was used to determine the stresses and finite displacements developed in two-dimensional (2D) elastic structures of arbitrary geometry and with constituent materials of different properties.

The mathematical bases of the finite element numerical models are published elsewhere (Hayashi, 2008). Usually, the finite element method (FEM), applied in the present work, is treated on the basis of the principle of virtual work. The work illustrates that the external work done by the virtual displacement equals the internal work done by virtual strain. Let us consider a definite element within a domain concerned as shown in Fig.1. When the small displacement $\overline{u}_1$, which is called a virtual displacement, is applied to distort the element without distressing the balance of the system, the external work is written as

$$W = (\overline{\mathbf{u}}^e)^T \mathbf{f}^e \text{ where } \overline{\mathbf{u}}^e = \begin{Bmatrix} \overline{\mathbf{u}}_1 \\ \overline{\mathbf{u}}_2 \\ \overline{\mathbf{u}}_3 \end{Bmatrix} \text{ and } \mathbf{f}^e = \begin{Bmatrix} \mathbf{f}_1 \\ \mathbf{f}_2 \\ \mathbf{f}_3 \end{Bmatrix}$$

While taking $\overline{e}$ as virtual strain derived from virtual displacement and **s** as stress, the strain energy of the element are given by

$$U = \int_S (\overline{\mathbf{e}})^T \mathbf{s}\, dS$$

According to the principle of virtual work, both must be equal.

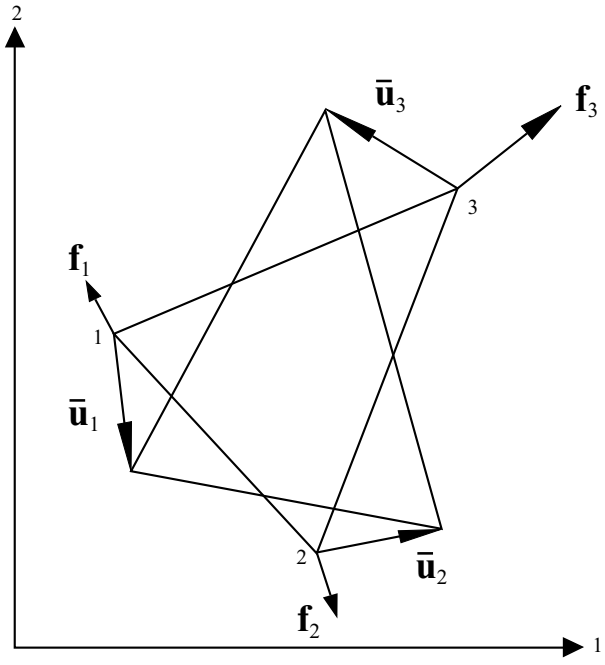

FIGURE 1 **Force vector and virtual displacement vector work at each nodal point in a certain finite element (after Hayashi, 2008).**

$W = U$

$$(\bar{\mathbf{u}}^{\mathbf{e}})^T \mathbf{f}^e = \int_S (\bar{\mathbf{e}})^T \mathbf{s}\, dS \quad (1)$$

Then, to obtain the practical form of (1), we assume the displacement within the element is a function of the coordinates. Since the simplest relation is linear, we use a linear relation as follows:

$$\begin{aligned} u &= a_0 + a_i x_i \\ &= a_0 + a_1 x_1 + a_2 x_2 \\ &= (1 \quad x_1 \quad x_2)\begin{bmatrix} a_0 \\ a_1 \\ a_2 \end{bmatrix} \\ &= \mathbf{ca} \end{aligned}$$

Substituting the values of the coordinates and displacements at nodes into this equation, we have

$$u_N = (1 \quad x_{N1} \quad x_{N2})\mathbf{a}$$

Written in vector form:

$$\mathbf{u}^e = \begin{bmatrix} u_1 \\ u_2 \\ u_3 \end{bmatrix} = \begin{bmatrix} 1 & x_{11} & x_{12} \\ 1 & x_{21} & x_{22} \\ 1 & x_{31} & x_{32} \end{bmatrix} \mathbf{a} = C\mathbf{a}$$

The coefficient vector **a** is derived from the equation,

$$\mathbf{a} = C^{-1}\mathbf{u}^e$$

$$\text{where, } C^{-1} = \frac{1}{\Delta}\begin{bmatrix} \Delta_{11} & \Delta_{21} & \Delta_{31} \\ \Delta_{12} & \Delta_{22} & \Delta_{32} \\ \Delta_{13} & \Delta_{23} & \Delta_{33} \end{bmatrix} \text{ and } \Delta \equiv \det C \text{ and } \Delta_{ij} \equiv \textit{cofactor of } C$$

Therefore, the inner displacement is represented in terms of nodal displacements.

$$u = \mathbf{c}C^{-1}\mathbf{u}^e = \frac{1}{\Delta}(\Delta_{11} + \Delta_{12}x_1 + \Delta_{13}x_2 \quad \Delta_{21}x_1 + \Delta_{22}x_2 + \Delta_{23}x_3 \quad \Delta_{31}x_1 + \Delta_{32}x_2 + \Delta_{33}x_3)\mathbf{u}^e$$

$$\text{Replacing with } \phi_N = \frac{1}{\Delta}(\Delta_{N1} + \Delta_{N2}x_1 + \Delta_{N3}x_2),$$
$$\text{we have } u = \phi_N \; u_N$$

Since we will consider a 2D situation, displacement has 2 components: u_1 and u_2.

$$u_1 = \phi_N \; u_{N1}$$
$$u_2 = \phi_N \; u_{N2}$$

Writing them in vector form,

$$\mathbf{u} = \begin{bmatrix} u_1 \\ u_2 \end{bmatrix} = \begin{bmatrix} \phi_1 & \phi_2 & \phi_3 & 0 & 0 & 0 \\ 0 & 0 & 0 & \phi_1 & \phi_2 & \phi_3 \end{bmatrix} \begin{bmatrix} \mathbf{u_1} \\ \mathbf{u_2} \end{bmatrix}$$

Then, exchanging the order of nodal displacements,

$$u_{11}u_{21}u_{31}u_{12}u_{22}u_{32} \Rightarrow u_{11}u_{12}u_{21}u_{22}u_{31}u_{32}$$

$$\mathbf{u} = \begin{bmatrix} u_1 \\ u_2 \end{bmatrix} = \begin{bmatrix} \phi_1 & 0 & \phi_2 & 0 & \phi_3 & 0 \\ 0 & \phi_1 & 0 & \phi_2 & 0 & \phi_3 \end{bmatrix} \begin{bmatrix} u_{11} \\ u_{12} \\ u_{21} \\ u_{22} \\ u_{31} \\ u_{32} \end{bmatrix}$$

$$= \Phi\mathbf{u}^e$$

Then, we can represent strain by nodal displacement as

$$e = \begin{bmatrix} e_{11} \\ e_{22} \\ 2e_{12} \end{bmatrix} = \begin{bmatrix} u_{1,1} \\ u_{2,2} \\ u_{1,2} + u_{2,1} \end{bmatrix} = \begin{bmatrix} \phi_{1,1} & 0 & \phi_{2,1} & 0 & \phi_{3,1} & 0 \\ 0 & \phi_{1,2} & 0 & \phi_{2,2} & 0 & \phi_{3,2} \\ \phi_{1,2} & \phi_{1,1} & \phi_{2,2} & \phi_{2,1} & \phi_{3,2} & \phi_{3,1} \end{bmatrix} \mathbf{u}$$

$$= B\mathbf{u}^e$$

$$\text{where } B = \frac{1}{\Delta}\begin{bmatrix} \Delta_{12} & 0 & \Delta_{22} & 0 & \Delta_{32} & 0 \\ 0 & \Delta_{13} & 0 & \Delta_{23} & 0 & \Delta_{33} \\ \Delta_{13} & \Delta_{12} & \Delta_{23} & \Delta_{22} & \Delta_{33} & \Delta_{32} \end{bmatrix}$$

As for the stress vector, according to the constitutive law of elasticity,

$$\mathbf{s} = \begin{bmatrix} \sigma_{11} \\ \sigma_{22} \\ \sigma_{12} \end{bmatrix} = D\mathbf{e}$$

For example, in the case of plane strain

$$\mathrm{D} = \frac{E(1-\upsilon)}{(1+\upsilon)\quad(1-2\upsilon)}\begin{bmatrix} 1 & \frac{\upsilon}{1-\upsilon} & 0 \\ \frac{\upsilon}{1-\upsilon} & 1 & 0 \\ 1 & 0 & \frac{1-2\upsilon}{2(1-\upsilon)} \end{bmatrix}$$

Then, according to the principle of virtual work,

$$(\bar{\mathbf{u}}^e)^T \mathbf{f}^e = \int_s (\bar{\mathbf{e}})^T \mathbf{s}\, dS$$
$$= (\bar{\mathbf{e}}^e)^T \left[\int_s B^T \quad DB \quad dS\right] \mathbf{u}^e$$
$$\mathbf{f}^e = K^e\mathbf{u}^e$$

This is called the stiffness equation of the element.

Superposing every all the stiffness equations of all the elements, we obtain the stiffness of the whole domain:

$$\mathbf{f} = K\mathbf{u}$$

If a body force ($\mathbf{f}_b$) is considered, the principle of virtual work must be modified as

$$(\overline{\mathbf{u}}^e)^T\left(\mathbf{f}^e - \int_S \mathbf{f}_b \quad dS\right) = \int_S (\overline{\mathbf{e}})^T \mathbf{s}\, dS$$

Fault analysis

The Mohr-Coulomb criterion has been successfully applied to the study of a number of structural geology and rock mechanics problems, such as fault/fracture growth in fold-thrust belts. Hayashi (2008) has incorporated the Mohr-Coulomb criterion into his FE software package. Failure of a mass of rock is controlled by stress applied to it. The Mohr-Coulomb failure envelope (Fig. 2) is based on a linear relationship between the shear stress $\boldsymbol{\tau}$ and the normal stress $\boldsymbol{\sigma}_n$:

$$\tau_{failure} = c + \sigma_n tan\phi \tag{2}$$

Where c is the cohesive strength of rock and $\boldsymbol{\phi}$ is the angle of internal friction. Failure occurs when the Mohr circle first touches the failure envelope. This occurs when the radius of the Mohr circle, $(\boldsymbol{\sigma}_1\text{-}\boldsymbol{\sigma}_3)/2$, is equal to the perpendicular distance from the center of the circle at $(\boldsymbol{\sigma}_1+\boldsymbol{\sigma}_3)/2$ to the failure envelope,

$$\left(\frac{\sigma_1-\sigma_3}{2}\right)_{failure} = c\,\cos\phi + \left(\frac{\sigma_1+\sigma_3}{2}\right)\sin\phi \tag{3}$$

According to Melosh and William (1989), the proximity to failure (P_f) is the ratio between the calculated stress and the failure stress, which is given by

$$P_f = \left[\frac{\left(\frac{\sigma_1-\sigma_3}{2}\right)}{\left(\frac{\sigma_1-\sigma_3}{2}\right)_{failure}}\right] \tag{4}$$

When the value of the ratio reaches one (P_f=1), failure occurs, but when P_f< 1 the stress is within the failure envelope and the rock does not fail. The proximity to failure P_f reveals which part of the model is close to failure or already failed by generating faults. The type of faulting has been determined by Anderson's theory (1951). According to his theory three classes of faults (normal, strike-slip, and thrust) result from the three principal classes of inequality that may exist between the principal stresses.

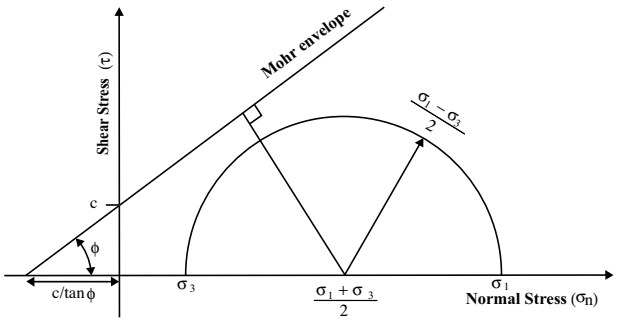

FIGURE 2 | **Failure envelope and Mohr's circle in $\sigma - \tau$ space. ϕ is the angle of internal friction (after Melosh and Williams, 1989).**

GEOLOGICAL SETTING OF THE STUDY AREA

The Andean belt extends for approximately 9000 km along the western margin of the South American continent. The physiography of Colombia (Fig.3) is dominated by the Andes Mountains in the west and the Amazon basin to the east. The Colombian Andes form three separate ranges: the Western Cordillera (WC), Central Cordillera (CC), and Eastern Cordillera (EC). The EC rises in southwestern Colombia, with a NE-SW strike, and reaches its maximum width at approximately 6^{O}N (up to 250 km). The Cauca Valley separates the Western and Central Cordilleras, and the Magdalena Valley separates the Central and Eastern Cordilleras. East of the EC is the Llanos Basin (Cooper et al., 1995). Megard (1987) interpreted that the Romeral suture is a series of discrete collisions commencing in the Early Cretaceous and ending in the Eocene. The suture between the Guyana shield and the Central Province is the Borde Llanero, which approximately coincides with the Llanos Foothills thrust front (Suarez, 1990).

The major tectonic events that influenced the development of the Colombian basins are all closely tied to the evolution of the active margin of western South America. The EC represents the leading edge of deformation in the northern Andes. In the northern portion, the structures related to the thrust faults have a NW-SE trend, in contrast with the overall NE-SW trend that characterizes most of the EC (Cooper et al., 1995; Corredor, 2003a). The basement of Colombia is divisible into three zones separated by major sutures:

1. The Precambrian Guyana shield in the east;
2. The Central Province of Precambrian-early Paleozoic metamorphic rocks, which underlies the Central and Eastern Cordilleras; and
3. Accreted oceanic crustal fragments and subduction related sediments and volcanics, which form the WC.

The basement of the EC is covered by a thick sequence of Mesozoic and Cenozoic sedimentary rocks. The sedimentary rocks were strongly deformed during the Neogene by thrusting and folding (Cooper et al., 1995; Vasquez and Altenberger., 2005).

The Maracaibo Basin is a topographic depression bounded to the east and south by the Medida Andes of Venezuela and to the west by the Sierra de Perija of Venezuela and Colombia. Both uplifted mountain blocks expose Paleozoic basement rocks and Mesozoic-Cenozoic carbonate and clastic rocks that were mainly folded and thrusted by regional shortening in the Paleozoic and late Neogene. The triangular-shaped Maracaibo block is enclosed by the left-lateral Santa Marta-Bucaramanga fault to the west in Colombia, and by the right-lateral Bocono fault to the east in the Merida Andes of Venezuela (Duerto et al., 2006).

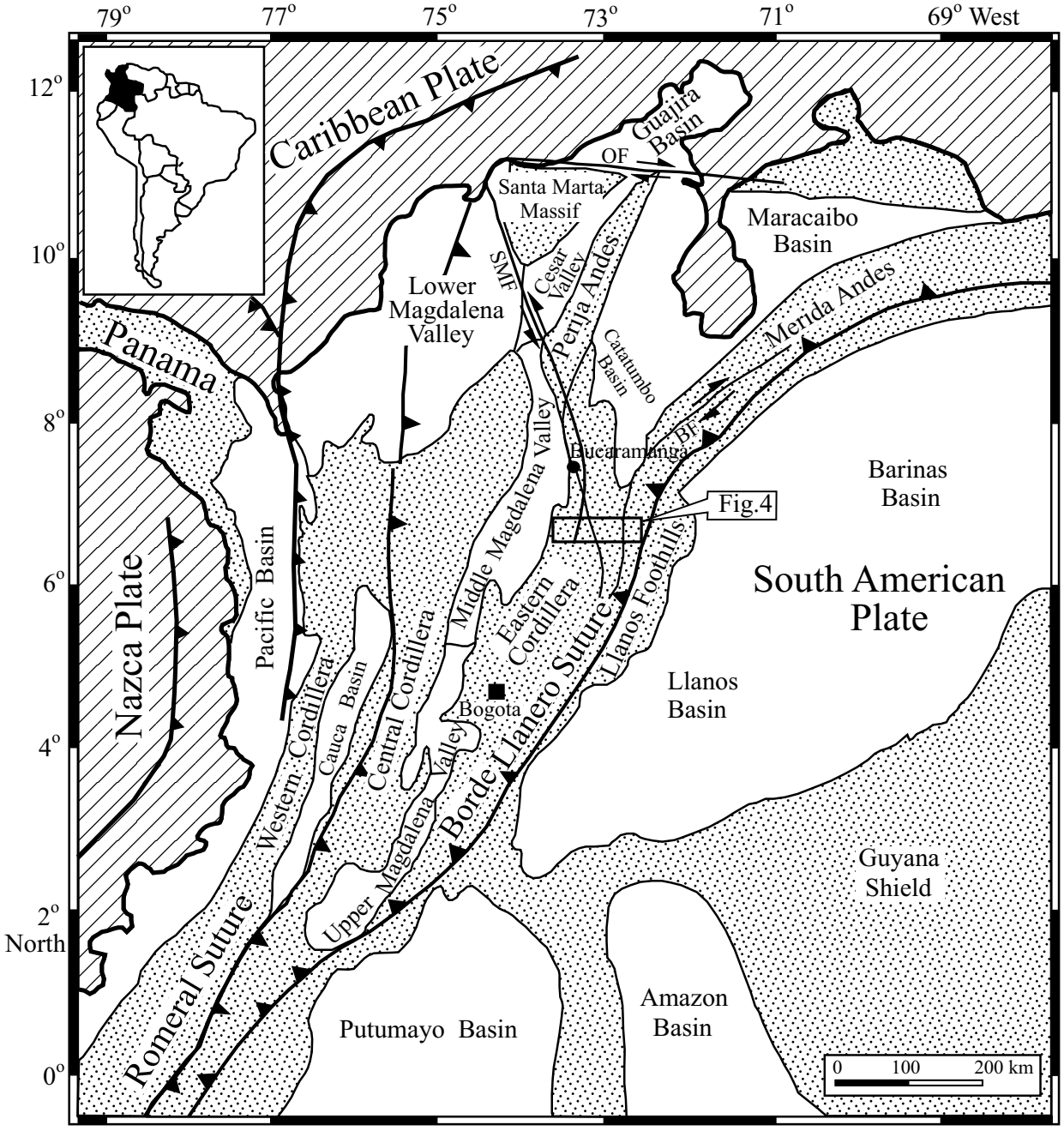

FIGURE 3 | **Map of major tectonic provinces of Colombia, with present-day sedimentary basins (shown in white) (compiled after Cooper et al., 1995; Ego et al., 1996). Abbreviation: BF = Bocono Fault, OF = Oca Fault. Dotted pattern corresponds to the Precambian basement in the foreland regions and to Paleozoic – Cenozoic rocks in the orogen. White corresponds mainly to Tertiary basins.**

MODEL

Model geometry

A 2D finite element model (FEM) was constructed based on a regional geological cross-section (Fig. 4B) of Corredor (2003a). The major tectonic features and the location of the profile are reported in Figs. 3 and 4A. The simplified model (Fig. 5A) is extended up to 173 km and consists of a 45 km thick continental brittle crust. The model consists of six layers, in which layer 3 represents pre-existing thrust faults within the basement, most of which are extended to the bottom at a depth of 45 km. The rest of the five layers 1, 2, 4, 5, and 6 correspond to individual crustal units based on density variations. This 2D vertical cross-section through the Andean crust has been represented by a finite element mesh composed of an assembly of 3000 triangular elements and 1596 nodes in plane-strain conditions.

Boundary conditions

In the modeled area, there is a contradiction regarding the influence of subducting plate and its relation to the deformation in the overriding plate. Deformation may be caused by either the Nazca plate (e.g., Pennington, 1981; Trenkamp et al., 2002; Corredor, 2003b) or the Caribbean plate (e.g., Ego et al., 1996; Cortes and Angelier, 2005; Iturralde and Lidiak, 2006a, 2006b; Giunta et. al., 2006; James, 2006; Pindel et al., 2006; Suter et al., 2008) moving with respect to the South American plate. In our NE-SW transect model, horizontal displacement caused by convergence of the Nazca plate has been considered as the prime driving force for the overriding crustal deformation of the South American plate. This assumption is reflected in the boundary conditions used. The grid and applied boundary conditions are shown in Fig. 5B. The upper part of the model represents Earth's surface and is free in all directions. The bottom of the grid is prevented from moving in the vertical (y) direction while a uniform

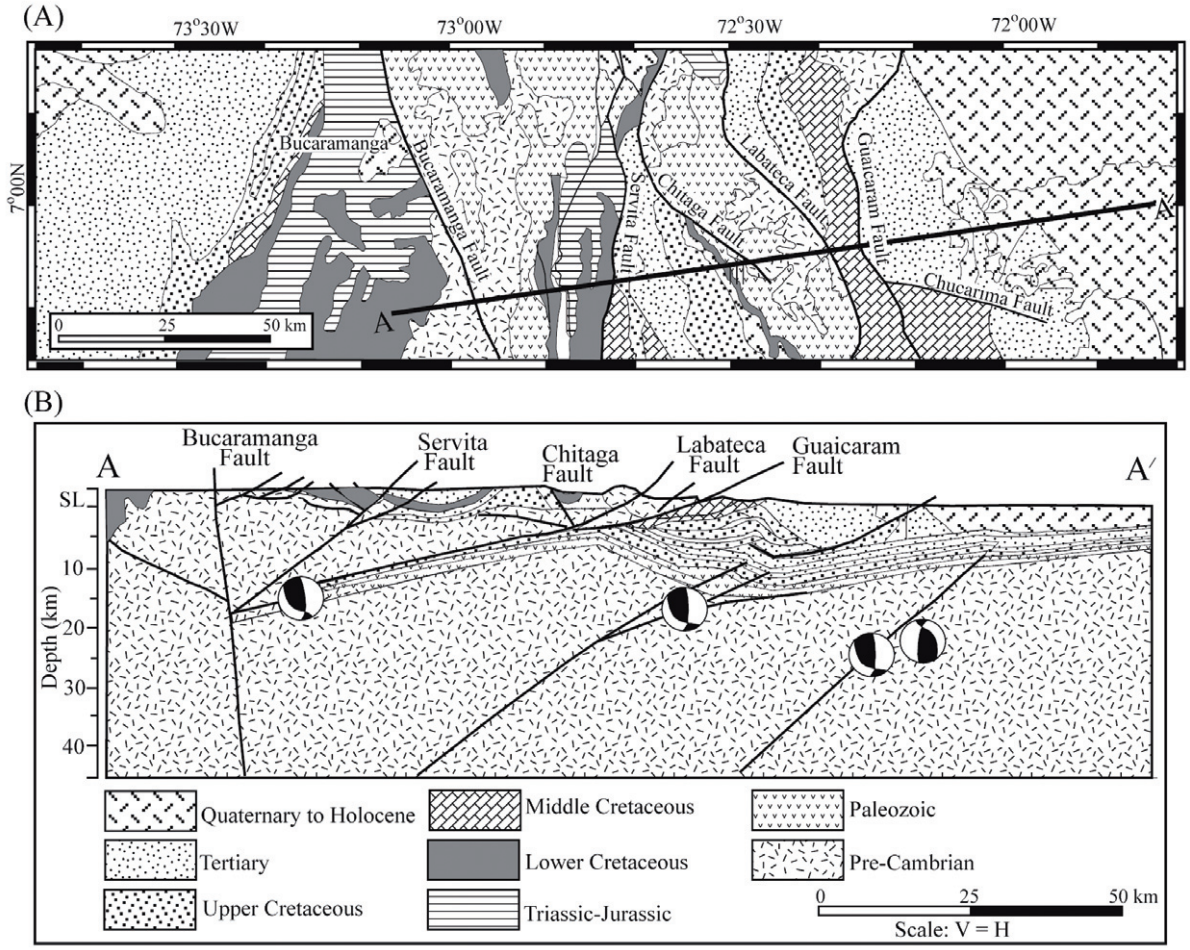

FIGURE 4 | **A) Compiled geologic map of the northern portion of the Eastern Cordillera of Colombia showing the main structural elements, the major stratigrapgic units and the location of the regional geologic cross-section A-A′. B) Regional balanced cross-section A-A′, which shows the present situation after 90 km of shortening occurred across the northern part of the Eastern Cordillera (modified after Corredor, 2003a).**

body force (gravity) is applied throughout. An equivalent horizontal nodal displacement has been applied along the left wall of the model. Free-slip boundary conditions have been used along the right wall of the model. The point marked with a triangle is fixed in the horizontal dimension and free in the vertical dimension. Displacement, designated by arrows, in the bottom (along x direction) is decreased linearly from the left side to the right.

Mechanical parameters of the model

In performing the FEM analysis, it is assumed that the geological materials involved are homogeneous and elastic, although it is certain that the geological rock-body must be regarded as visco-elastic, as already mentioned by Hayashi (1972) and others. In our model, the crust up to 45 km is assumed to behave as an elastic material because brittle characteristics of basement rocks generate thick-skinned faults up to 45 km in depth. In addition, the presence of earthquakes and the results of faulting (Corredor, 2003a) inferred in Fig. 4B make it possible to assume an elastic behavior.

We have divided the whole model into six layers, which represent litho-structural sequences from top (Quaternary) to bottom (Pre-Cambrian basement), shown in Table 1. The five rock-mechanical parameters for individual rock layers—density, Poisson's ratio, Young's modulus, friction angle, and cohesion—used in experiments are listed in Table 2. Regional longitudinal seismic velocity and crustal density have been considered here because of the lack of proper seismic sections along the modeled area. The crustal density was obtained from a 2D Andean crustal gravity-seismic model from Introcaso et al. (1992). The average values of density of different rock layers ranged from 2800 kg/m^3 to 2680 kg/m^3. The mean P-wave velocities ranged from 6.3 km/s to 5.0 km/s for rigid to moderate rock layers, respectively. The generalized value of Poisson's ratio used in the model is 0.25. Young's modulus ranged from about 93 to 15 GPa, which were calculated using the following equation (Timosenko and Goodier, 1970) in accordance with the homogeneity of rock rheology. In the case of Young's modulus values, 80% of the total calculated value has been applied for all layers except layer 2.

$$E = \rho V_p^2 \frac{(1+\nu)(1-2\nu)}{(1-\nu)} \quad (5)$$

Where E= Young's modulus, V_p = P-wave velocity, p = density and ν = Poisson's ratio. The two other physical parameters, internal friction angle φ and cohesion c, have been obtained from Clark (1966). Parameters of all experiments (from 1 to 12) are summarized in Table 3.

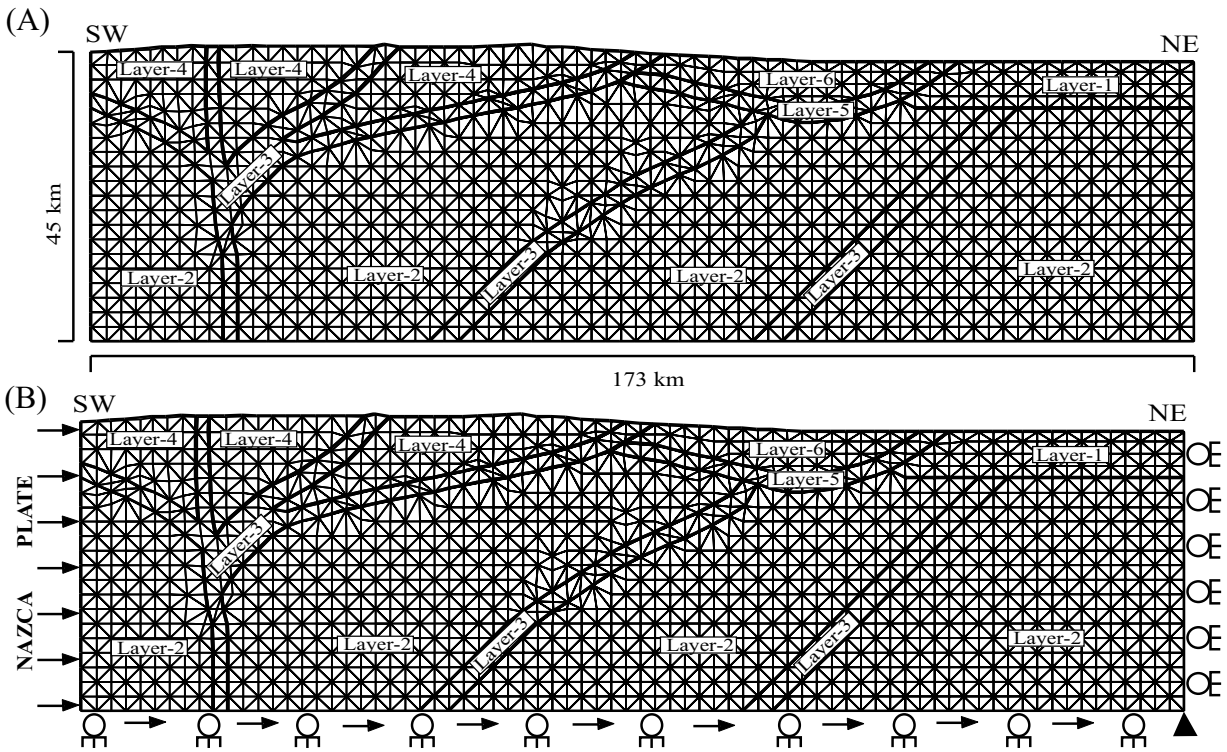

FIGURE 5 | **A) Simplified geometry, proposed layers and finite element mesh of the model. The mesh is composed of 3,000 plane-strain triangular elements and 1,596 nodes. B) Boundary conditions (see details in text) of the model.**

TABLE 1 | **Proposed layers, stratigraphy, and major rock types for the proposed modeling. * Marks in Layer-3 indicate pre-existing basement faults.**

Layers	Stratigraphy	Prime rock types
6	Quaternary, and Tertiary	Alluvium deposits and colluvium
5	Tertiary, and upper Cretaceous	Non-marine, coarse-grained, and mostly red siliciclastic sequence
4	Tertiary	Non-marine, coarse-grained, and mostly red siliciclastic
	Cretaceous	Marine carbonate and siliciclastic sequence [2].
	Triassic Jurassic	Volcaniclastic, and plutonic basement
	Pre-Cambrian Basement	High-grade metamorphic rocks and granitoid intrusions
3*	------	Basement with slickenside materials especially Gypsum
2	Pre-Cambrian Basement	High-grade metamorphic rocks and granitoid intrusions
1	Quaternary	Alluvium deposits and colluvium

TABLE 2 | **Rock-mechanical parameters used in finite element modeling. Abbreviations: L = layers, ρ = density Vp = Primary wave velocity v = Poisson's ratio; E = Young's modulus; c = cohesion Clark, 1966); ϕ = angle of internal friction (deg.) (Clark, 1966).**

Layers	ρ (kg/m^3)	V$_p$ (km/s)	v	E (GPa)	c (MPa)	ϕ (deg.)
L – 1	2680	5	0.25	54	25	20
L – 2	2800	6.3	0.25	93	50	35
L – 3	---	---	0.25	15	25	15
L – 4	2700	5.5	0.25	68	40	35
L – 5	2680	5.3	0.25	63	30	20
L – 6	2680	5.2	0.25	60	30	20

TABLE 3 | **Rock-layer properties (c, and ϕ) applied for parametrical tests (Figures 7 to 9). Abbreviations: c = cohesion (MPa); ϕ = angle of internal friction (deg.); L = layer of the model. Star remarking (*) values were taken from Clark (1966).**

Experiment No	Varying Parameters	L-1	L-2	L-3	L-4	L-5	L-6	Fig.
1	c (*) (Table 2)	25	50	25	40	30	30	7A
	ϕ (*) (Table 2)	20	35	15	35	20	20	
2	c +5	30	55	30	45	35	35	7B
	ϕ +5	25	40	20	40	25	25	
3	c +10	35	60	35	50	40	40	7C
	ϕ +10	30	45	25	45	30	30	
4	c +15	40	65	40	55	45	45	7D
	ϕ+15	35	50	30	50	35	35	
5	c +5	30	55	30	45	35	35	8A
	ϕ (*)(Table 2)	20	35	15	35	20	20	
6	c +10	35	60	35	50	40	40	8B
	ϕ (*)(Table 2)	20	35	15	35	20	20	
7	c -5	20	45	20	35	25	25	8C
	ϕ (*)(Table 2)	20	35	15	35	20	20	
8	c -10	15	40	15	30	20	20	8D
	ϕ (*)(Table 2)	20	35	15	35	20	20	
9	ϕ +5	25	40	20	40	25	25	9A
	c (*) (Table 2)	25	50	25	40	30	30	
10	ϕ +10	30	45	25	45	30	30	9B
	c (*) (Table 2)	25	50	25	40	30	30	
11	ϕ -5	15	30	10	30	15	15	9C
	c (*) (Table 2)	25	50	25	40	30	30	
12	ϕ	10	25	5	25	10	10	9D
	c (*) (Table 2)	25	50	25	40	30	30	

MODELING RESULTS

The modeling results presented here are based fundamentally on: 1) distributions, orientations, and magnitudes of principal stresses; 2) shear stress distribution; and 3) proximity of failure of elements. Some parametric tests have been incorporated to recognize the role of cohesion and friction angle along the fault zones. The applied convergent displacement in the modeling is 1000 m for all experiments.

Stress distribution

The spatial distributions of stress with its orientations and magnitudes are shown in Fig. 6A, where σ1 is the maximum compressive stress, and σ3 is the minimum compressive stress, aligned along the horizontal and vertical arms, respectively. The displacement boundary conditions selected in this scenario imply an overall orientation of σ1 in the horizontal direction in most of the uppermost crust. Stresses in the model's upper crust are much more uniform in orientation and reflect the overall horizontal compressional setting. Although the stress values may change with different material properties, the stress pattern will remain the same. In all the cases of our modeling, tensional failure

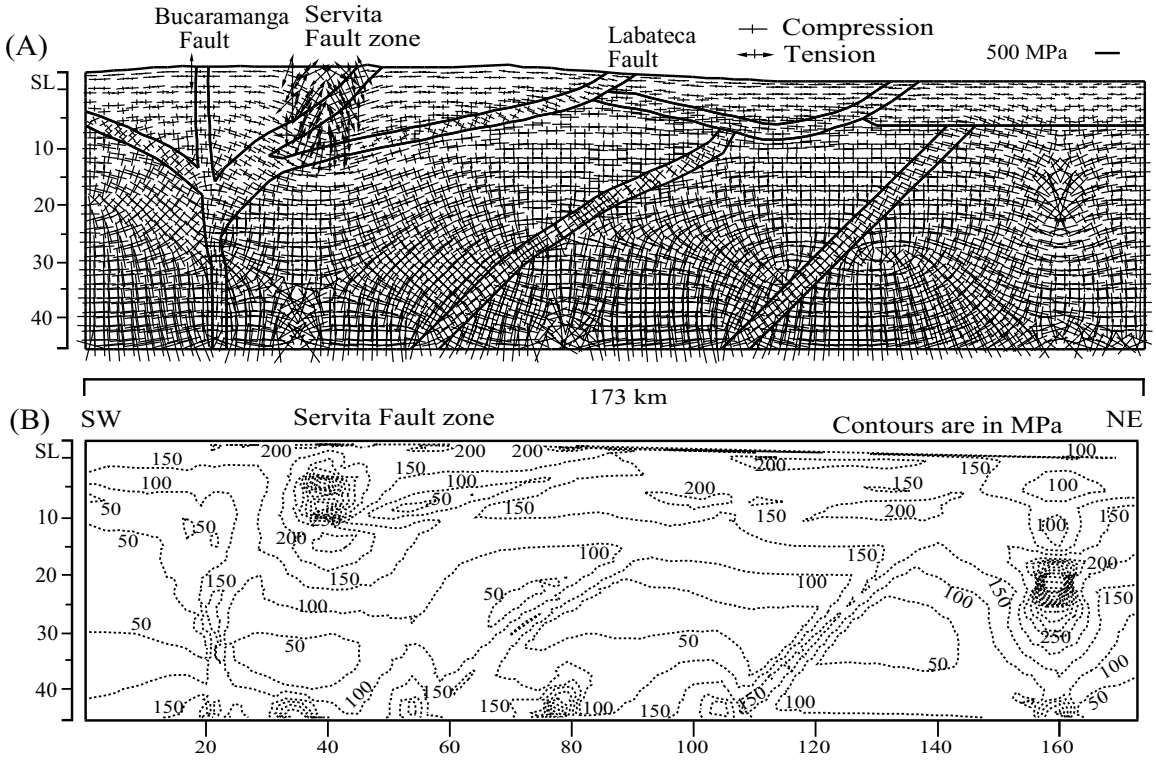

FIGURE 6 | **A) Distributions, orientations and magnitudes of principal stresses (σ_1 and σ_3). B) maximum shear stress (τ_{max}) distribution of the model.**

around the Servita and Bucaramanga fault system is very common. Regarding the results of the stress within the basement layer (layer-2) of the model, some significant stress reorientations occurred in the lower part of the model with respect to the sedimentary cover and upper part of the basement. This is explained in terms of variations of the elastic parameters assigned to the basement blocks. In general, the effect of mechanical boundaries is most significant if they create a small angle with respect to the general stress field. Small-scale changes of orientation in stress field, over distances of a few hundreds of kilometers, indicate complex tectonic process.

Shear stress distribution

Fig. 6B illustrates the distribution of maximum shear stress. τ_{max} is highly concentrated on the pre-defined fault-effect zones. High τ_{max} contours occurred where weak rheologies (layer 3) are located next to strong rheologies (layer 2). Barely adequate reactivation and differential movement occurred within layer 2. The prominent high τ_{max} zones cutting through the basement (layer 2) of the model are genetically related to the reactivation of faults. The τ_{max} distribution is highly variable and maximum deformation in the upper part of the model is achieved through a broad zone under the Servita Fault and Bukaramanga fault systems.

Proximity of failure of elements

To simulate fault zones, we have considered two main factors: a) the geometry, and b) the mechanical properties of fault zones. The effect of fault geometry is important because it concerns the dimension and structure of a fault zone and the fragmentation of the rupture surface, as well as the complexity of the fracture network. The contribution of each of the physical parameters (as shown in Table 2) controlling dynamic fault weakening and fault evolution depends on the values of the two main physical parameters, such as cohesion and friction angle.

In the present study, the crustal deformation is examined based on the proximity of failure of elements. Here failure of elements is influenced by two important rock-mechanical parameters: cohesion and angle of internal friction. As mentioned in the previous section, we have considered the Mohr-Coulomb failure criterion concept of proximity to failure of elements. Twelve numerical experiments differing in the cohesion and angle of internal friction (Table 3) are studied to examine the adoptability of elastic rock-mechanical properties for fault development. Values marked with a star (*) were taken from Clark (1966) (Table 2). We then manipulated our experiments with an interval of *values ± 5 (Table 3).

Simulated results (Figs. 7 to 9) corresponding to failure of elements occurred primarily within pre-defined thrust zones.

We have obtained a good consistency of failure of elements with the geometry of the fault-affected zones (Fig. 7A) when cohesion and angle of internal friction are the

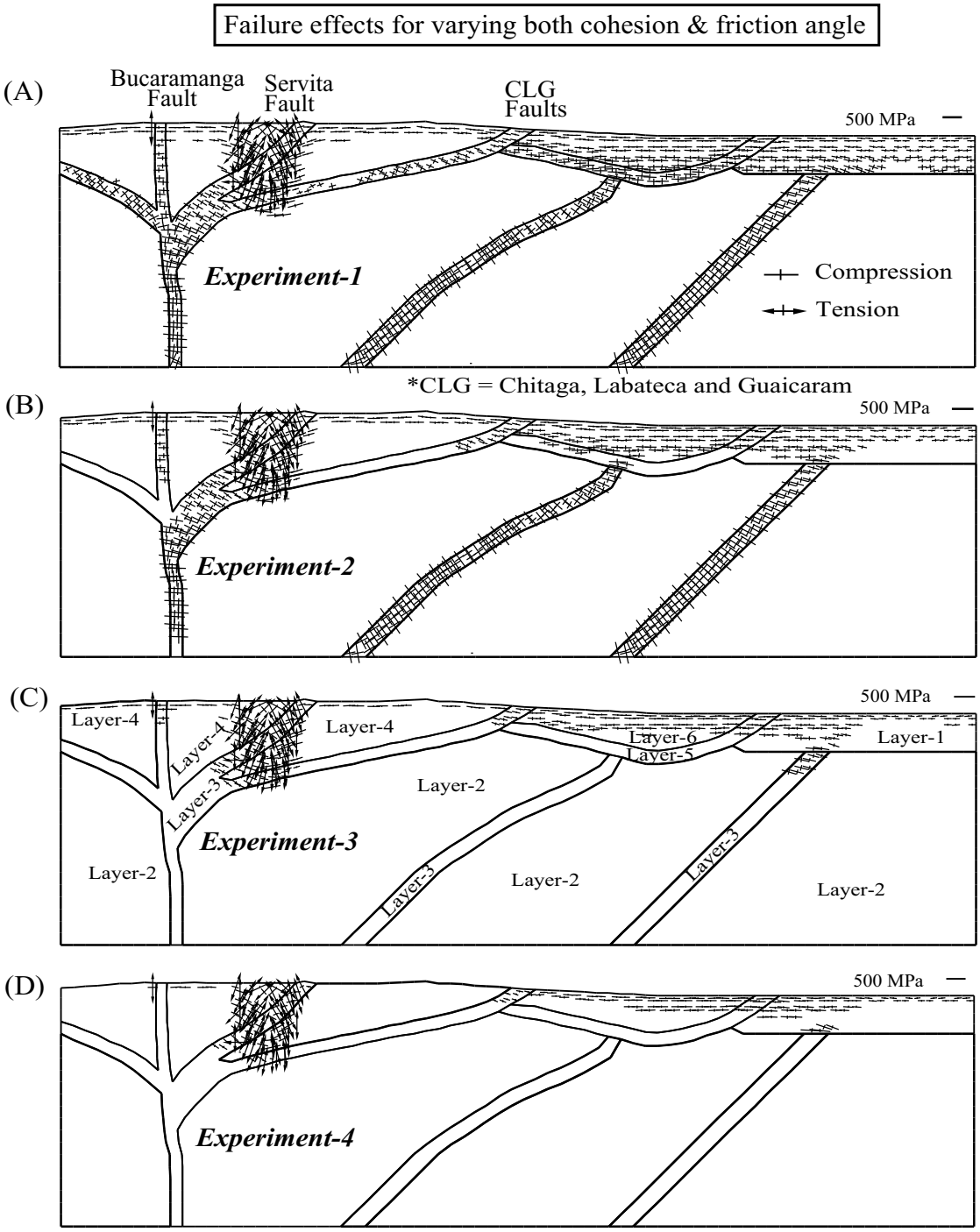

FIGURE 7 | **Parametrical tests of cohesion and angle of internal friction, where A) shows a good consistency of failure of elements within the geometry of fault-affected zones, B) shows that proximity of failure of elements decreases progressively with increasing both parameters (c+5, and ϕ+5) (see in Table 3). C) and D) show dramatic changes of failure (that rapidly decreases) of elements within fault-affected weak zone (Layer-3), with increasing cohesion and angle of internal friction (see in Table 3). But, there is no significant change of failure in elements within the Servita Faults system.**

same as in experiment-1 (Table 2 and 3). It is shown that modification of these parameters is mainly related to the transition state of evolution. The increase of both the cohesion and friction angle results in decreases in proximity of failure of elements within the layers (Fig. 7B-D). It is reasonable to conclude that when only cohesion is increased, an insufficient number elements fail within layer 3 (Fig. 8A-B), but when the friction angle is increased, there is a dramatic change in failure proximity, i.e., failure gradually decreases with increasing parameter values (Fig. 9A-B).

On the contrary, the decrease in these parameters favors a forward propagation sequence (Fig. 8C-D and

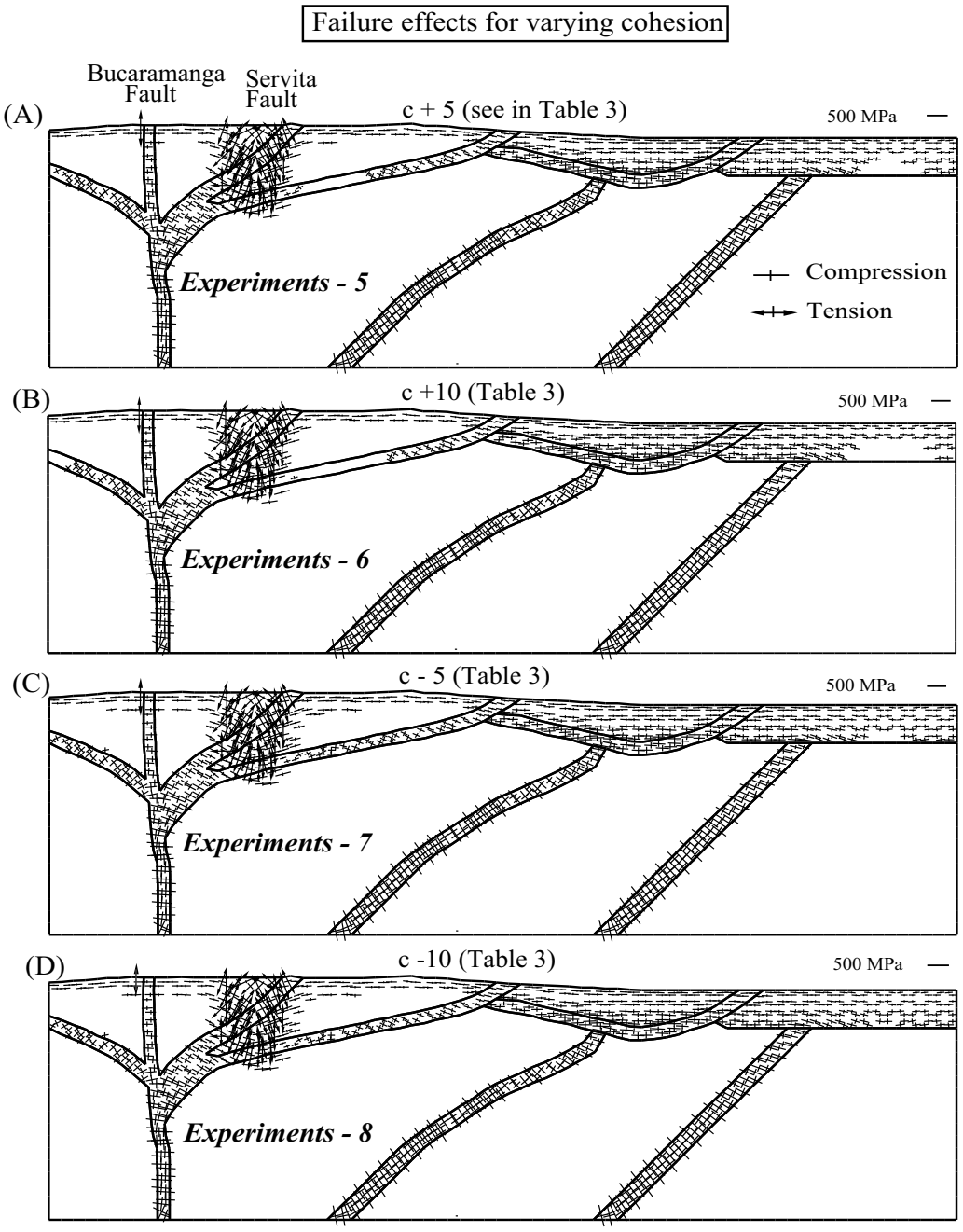

FIGURE 8 | **Proximity of failure of elements within layers due to effect of varying cohesion c. In this case, angle of internal friction (ϕ) remains constant as obtained from Clark (1966) (see Table 3). The increase of cohesion (shown in A and B) decreases in proximity of failure of elements within fault-affected layer. On the contrary, the decrease in parameter (shown in C and D) favors a forward propagation sequences. No significant changes of failure in elements are observed in and around the Servita and Bucaramanga Faults systems.**

Fig.9C-D). Therefore, comparison among all experiments (Figs. 7 to 9) demonstrates that cohesion and angle of internal friction of the basement are most important for controlling the reactivation of faults. Friction angle in particular plays a vital role in controlling fault geometry. The increase in values reduces reactivation on the innermost thrusts. It is interesting to remark that there is no variable impact of tensional failure in elements in the Servita half-graben area (Figs. 7 to 9) and Bucaramanga fault zone, while cohesion and angle of internal friction are variable. For all parametric experiments, it is obvious that tensional failure is entirely constant. This

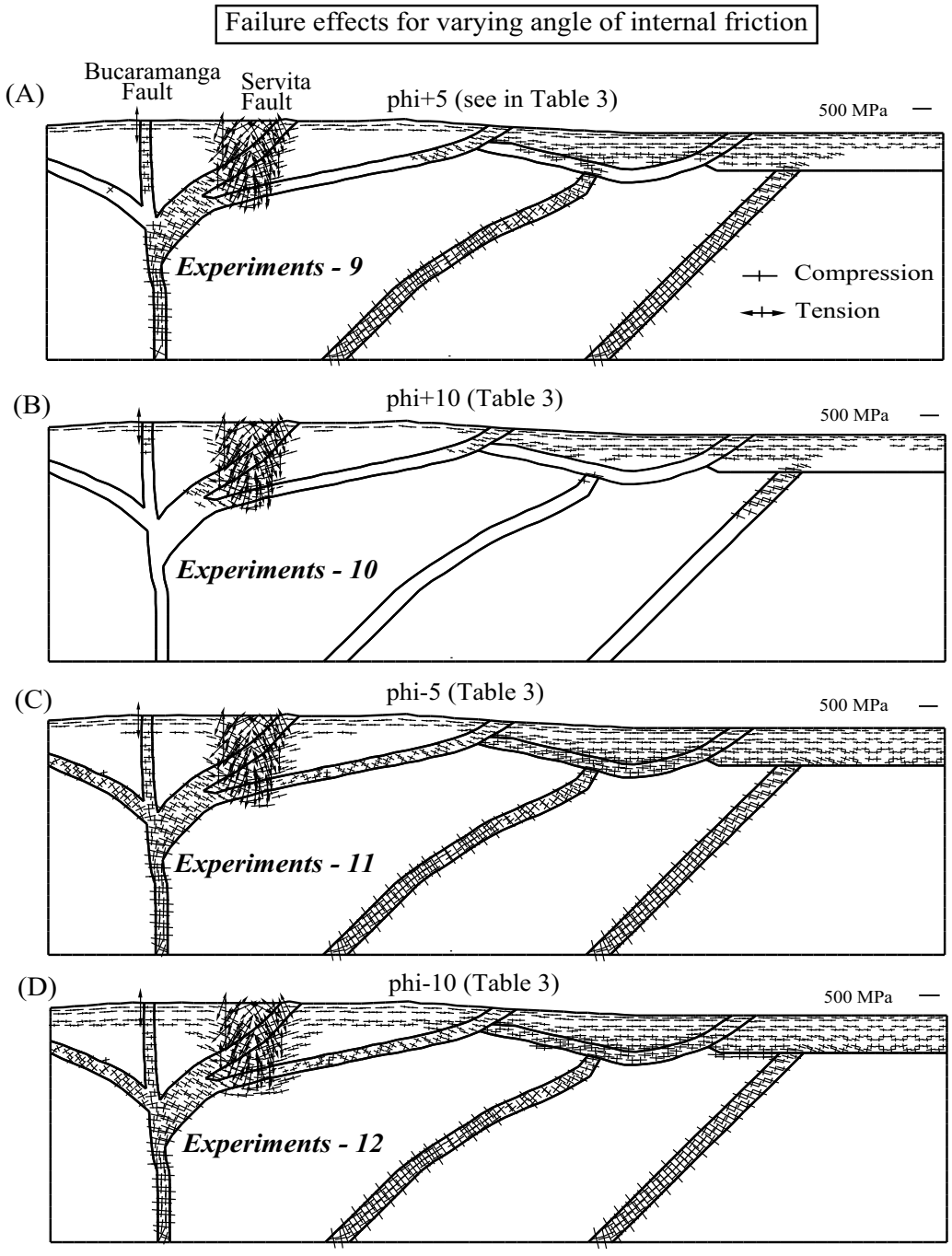

FIGURE 9 | **Proximity of failure of elements within layers due to effect of varying angle of internal friction (ϕ). In this case, cohesion c remains constant as obtained from Clark (1966) (see Table 3). The increase of angle of internal friction (shown in A and B) decreases in proximity of failure within fault-affected layer. On the contrary, the decrease in parameter (shown in C and D) favors a forward propagation sequences. No changes of failure of elements occur in and around the Bucaramanga and Servita Fault systems.**

may be due to the geometry of the fault and high topographic effect.

DISCUSSION

Historical evidence for extensional/rift tectonics in the northern Andes

Extensional tectonics are historically documented in the southernmost Andes (Klepeis and Austin, 1997), south central Andes (Carrera et al., 2006; Alonso et al., 2008), and central Andes (Richardson and Coblentz, 1994). This is also well studied in the northern Andes. For example, in northern Venezuela and Colombia, E-W, and NW-SE directed shortening led to the late Miocene-Pliocene inversion of Upper Jurassic normal faults and rifts, as well as the Andean orogeny or regional topographical uplift of the northern Andes (Duerto et al., 2006). During the Triassic, Jurassic and earliest Cretaceous, Colombia was peripherally affected by rifting related to eventual separation of North and South America in the proto-Caribbean (Jaillard et al., 1990; Duerto et al., 2006). Maze (1984) proposed an alternative mechanism for the extension in the back-arc region in Colombia, which, given the oblique nature of the subduction zone, may have had a transtensional component. McCourt et al. (1984) concluded that Early Cretaceous extension and subsidence may have been due to back-arc stretching behind the subduction zone off the western coast of South America. According to Butler and Schamel (1989) major deformation of the EC resulted from Panama's collision with South America. During this deformation phase, the EC was uplifted and eroded. Old extensional faults were inverted and new compressional structures developed. On the western flank of the EC and in the Magdalena valley, middle Eocene folds were reactivated. In contrast, shortening in the Neogene period preferentially deformed previous thin and weak rifted areas during northwest-southeast shortening and underthrusting of Caribbean oceanic crust and oceanic plateau crust beneath the continental crust of northern South America. Regional shortening by inversion and uplift of older rift structures is consistent with the highly elevated and elongated pop-up structures of the Merida Andes, Perija Andes, and Colombian Andes (Taboada et al., 2000; Colmenares and Zoback, 2003). The faults in the Colombian Andes (Fig. 4B) such as Servita fault, Chitaga fault, Labateca fault, and Guaicaram fault, are reactivated as thrusts, whereas Bucaramanga fault is reactivated as strike-slip fault (Corredor, 2003a). Thus, our present modeling results, including locations of extensional stresses, coincide with the past historical evidence.

Extension contemporaneous with thrusting in Andean orogenic belt

A characteristic feature of many convergent plate margins, especially those affected by the subduction of old, dense, oceanic crust, is the development of back-arc basins resulting from extensional tectonics (Molnar and Atwater, 1978). Extension may occur contemporaneous with, and parallel to, the direction of regional bulk shortening in an orogenic belt. Extensional structures formed both during and following regional contraction can coexist along the same cross section of the orogen (Jolivet and Goffe, 2000). For example, in our modeling section, the local formation of the normal shear zone striking parallel to the thrust has been described by Colmenares and Zoback (2003). Moreover, areas of extension may alternate with areas of contraction during block rotation between transcurrent faults at an active margin. Local contractional or extensional sites also formed because of changes in strike-slip of transcurrent ductile shear zones in the deep crust (Harris et al., 2002).

Extensional stresses in our model

There are two types of hypothesis regarding extensional tectonic of the Colombian EC. The first is intracontinental rifting related to the break up of Pangea that occurred during Triassic and Early Cretaceous times. The second holds that backarc extension occurred behind a subduction-related magmatic arc. This hypothesis suggests that the study area was located at the margin of the continent when active subduction of oceanic plates was occurring (Sarmiento et al., 2006). The present study shows that extensional deformation in the fold-and-thrust belt of the Colombian EC is linked with plate convergence, and geometry of fault, and topographic effects. In the southernmost Andes and the central Andes, there are two prominent reasons that have been recognized for the extension in the crust. The first is the inclination of the thrust fault (Klepeis and Austin, 1997; Islam and Hayashi, 2008a; 2008b), and the second is topographic and gravitational effects (Richardson and Coblentz, 1994; Islam and Hayashi, 2008a; Islam and Hayashi, 2008b). Klepeis and Austin (1997) stated that sub-horizontal thrusts faults in the southernmost Andes are characterized by shortening, whereas sub-vertical thrusts faults are characterized by extension. Results of Islam and Hayashi (2008b) match up with Klepeis and Austin (1997). In the northern Andes, where our modeling section is located (Fig. 4B), the Bucaramanga fault is almost vertical, whereas the Servita fault is close to sub-vertical, and other faults such as Chitaga fault, Labateca fault, and Guaicaram fault show less inclination. Servita fault is related to the development of a half-graben type basin (Corredor, 2003a). Usually, the inclination of fault, which is related to the development of regional half-graben type basin, is more than 60°. According to Melosh and Williams (1989), prior to the development of a half-graben type basin an extending elastic layer first fails on a normal fault, which cuts the layer with a dip of approximately 60° in accordance with Anderson's (1951) theory of normal faulting. Slip along this fault flexes the adjacent rock layers until new fault forms where the fiber stresses

induced by bending are most extensional. Our modeling results reveal that extensional stresses are concentrated in and around the Servita half-graben and Bucaramanga Fault systems, where thrust angle may be privileged to cause tensional failure. The gravitational effects due to high topography may be the second major reason for the upper crustal extension. Thus, our calculated result shows good agreement with the study of Klepeis and Austin (1997), Richardson and Coblentz (1994), Carrera et al. (2006), Alonso et al., (2008), Islam and Hayashi (2008a); Islam and Hayashi (2008b).

Some extensional mechanisms: 1) block escape, 2) slab retreat, 3) post-orogenic collapse, 4) under-thrusting/underplating and wedge extension, 5) lower crustal extrusion, and 6) traction reversal, are proposed by Willett (1999). These mechanisms generate extensional regimes in convergent orogens. In the present analysis, we emphasized that the extension is possibly associated with intra-continental stress adjustment following the under-thrusting/under-plating (e.g., Fig. 10A) of the Caribbean plate beneath the South American plate (Fig. 10B). Under-thrusting (Fig. 10A) is one of the important mechanisms of extensional deformation under the convergence environment. In this case, extensional deformations at shallow levels in an accretionary wedge are driven by tectonic underplating, or transfer of accreted mass across a deep decollement at the base of the deforming wedge (Willett, 1999). Our modeling result demonstrates that extensional deformation along fold-and-thrust belt of the EC may be related to a geometry similar to that shown in Fig. 10A (Willett, 1999). This is supported by the 2D model (Fig. 10B) of Cortes and Angelier (2005), where the Caribbean plate, along 7°N, is underplating below the northern Andes and the high convergence of the NE-moving Nazca plate, play a vital role in driving the base of the deforming wedge of the overriding South American Plate.

Comparison with focal mechanism solution

The stress pattern and dominant style of deformation in our model were compared with earthquake focal mechanisms. The deformation of the modeled area is mainly brittle, and is located near the thrust planes for all major thrusts. This result is in good agreement with focal mechanism solu-

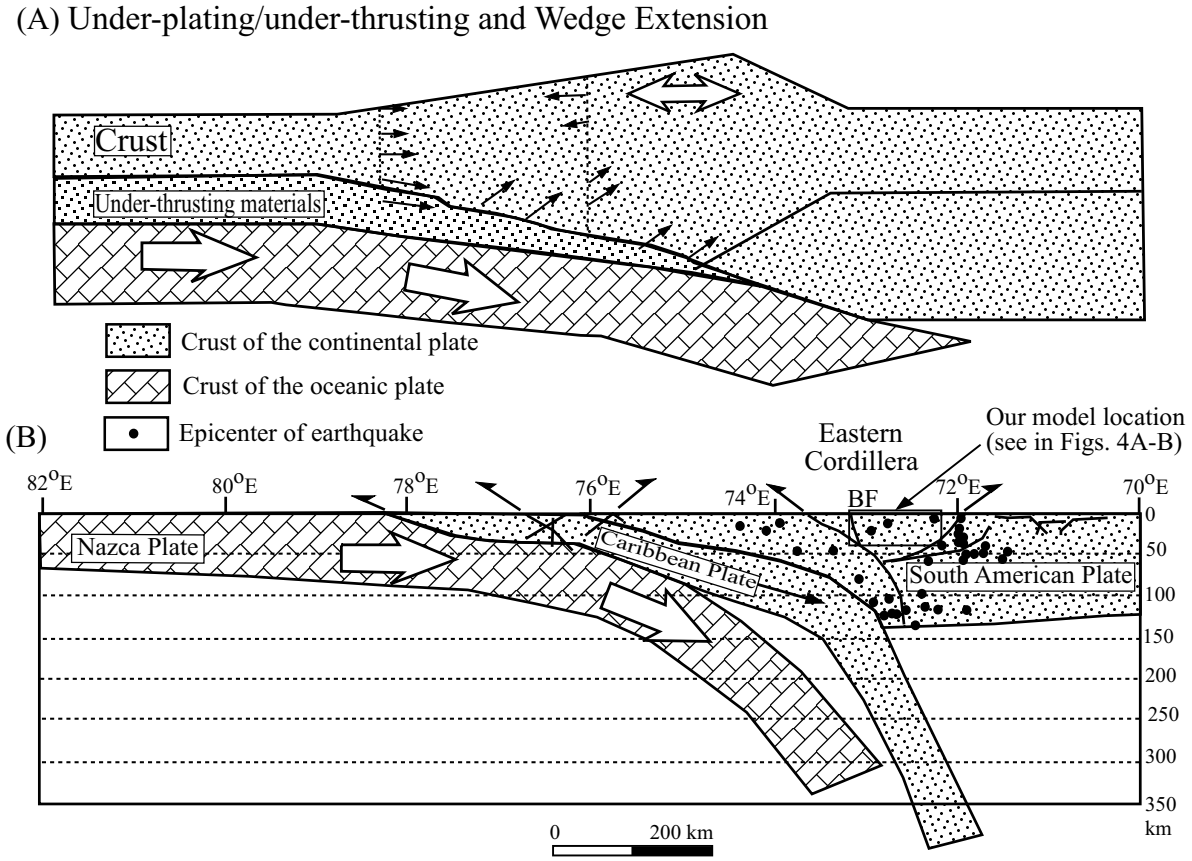

FIGURE 10 | **A) Model of extension developed under overall convergent environments. Double arrow indicates region of crustal extension (after Willett, 1999). B) Cross-section along 7°N showing the geometry of the Caribbean and Nazca plate slabs below the northern Andes (modified after Cortes and Angelier, 2005). BF = Bucaramanga Fault.**

tions (Fig. 4B). A final indication of basement deformation is the location of thrusting earthquakes in the basement. Some events are shown in Fig. 4B (Corredor, 2003). The distribution of these events and their focal mechanisms are both consistent with distributed compression stresses of the basement. Most of the deformation is observed in narrow shear zones of pre-existing faults when τ_{max} is 150 MPa (Fig. 6B). This means that the present-day basement deformation and seismicity of the EC fold-and-thrust belt are caused by shear stresses of no less than 150 MPa. According to Colmenares and Zoback (2003), and (Zoback, 1992) the stress direction in the EC of Colombia shows maximum compression trending approximately E-W. The stress field is compressional: the majority of earthquakes are characterized by thrust faulting (with some strike-slip faulting). Two earthquakes due to normal faulting (Fig. 11) are thought to be associated with

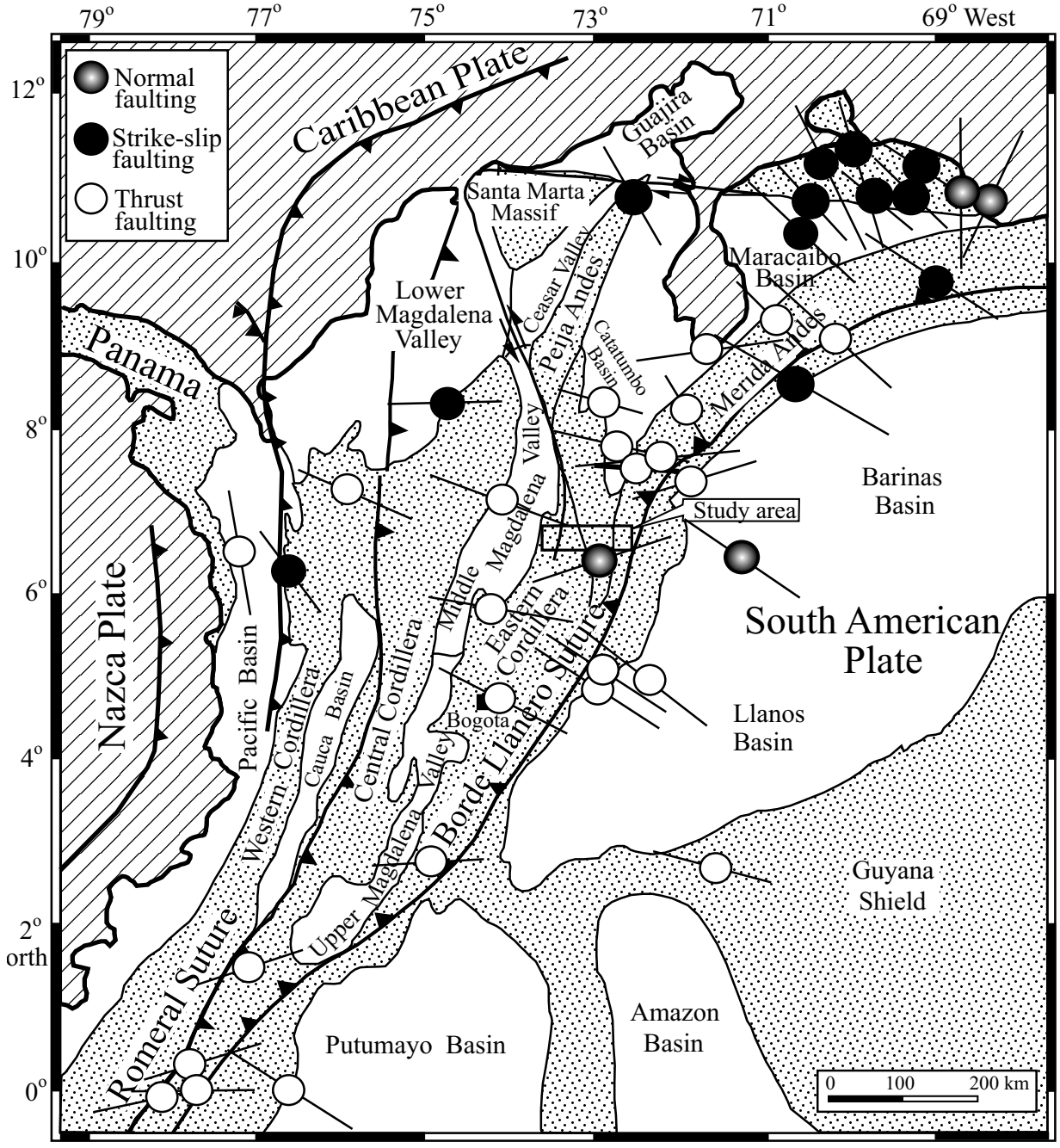

FIGURE 11 | **The present-day focal mechanism data of the Colombian Andes are taken from Colmenares and Zoback (2003). Major tectonic provinces are same as shown in Figure 3 (Cooper et al., 1995; Ego et al., 1996).**

the high topography of the Andes. Thus, extensional stresses as found in our modeling are also consistent with the high topography.

CONCLUSIONS

In this numerical modeling study, the present-day state of stress along the fold-and-thrust belt of the Colombian EC has been discussed. The rational states of stress have been recognized primarily through studying rock-mechanical properties, geometry of the faults, and historical evidence.

Extensional stresses in the Andean orogenic belt are historically documented and our present modeling result corroborates this history. The tensional failure of elements that occurred in and around the Servita and Bucaramanga fault systems supports the results of both the geometry of the fault and gravitational effects along the fault.

Relying upon the evaluation of stress measurements, it is reasonable to conclude that extensional stresses within upper crustal thick-skinned portions of the Colombian EC fold-and-thrust belt are still active, although the Northern Andean Block is located within a contractional orogenic belt.

ACKNOWLEDGMENTS

The Ministry of Education, Culture, Sports, Science and Technology (Monbukagakusho) of Japan is acknowledged for its financial support of the first author. The Editor, Professor Dr. Lluís Cabrera, Dr. Giorgi Khazaradze, and an anonymous reviewer are thanked for their helpful comments and corrections to an earlier version of the manuscript.

REFERENCES

Alonso, J.L., Gallastegui, J., Sansegundo, J.G., Farias, P., Fernández, L.R.R., Ramos, V.A., 2008. Extensional tectonics and gravitational collapse in an Ordovician passive margin: The Western Argentine Precordillera. Gondwana Research, 13, 204–215.

Anderson, E.M., 1951. The Dynamics of Faulting and Dyke Formation with Application to Britain. Edinburgh, Oliver & Boyd, 2nd edition, 133pp.

Butler, K., Schamel, S., 1989. Upper Crustal control of deformation and hydrocarbon traps along the Upper Magdalena Valley, Colombia (abstract). American Association of Petroleum Geologists - AAPG Bulletin, 73, 339p.

Caiazzo, C., Ascione, A., Cinque, A., 2006. Late Tertiary–Quaternary tectonics of the Southern Apennines (Italy): New evidences from the Tyrrhenian slope. Tectonophysics, 421, 23–51.

Carrera , N., Muñoz, J.A., Sàbat, F., Mon, R., Roca, E., 2006. The role of inversion tectonics in the structure of the Cordillera Oriental (NW Argentinean Andes). Journal of Structural Geology, 28, 1921-1932.

Charrier, R., Baeza, O., Elgueta, S., Flynn, J.J., Gans, P., Kay, S.M., Munoz, N., Wyss, A.R., Zurita, E., 2002. Evidence for Cenozoic extensional basin development and tectonic inversion south of the flat-slab segment, south Central Andes, Chile (33º-36ºS. L.). Journal of South American Earth Sciences, 15, 117-139.

Clark, Jr., S. P. (ed.), 1966. Handbook of Physical Constants. New York, The Geological Society of America, Memoir, 97, 587 pp.

Colmenares, L., Zoback, M.D., 2003. Stress field and seismotectonics of northern South America. Geology, 31, 721-724.

Cooper, M.A., Addison, F.T., Alvarez, R., Coral, M., Graham, R.H., Hayward, S.H., Martinez, J., Naar, J., Penas, R., Pulham, A.J., Taborda, A., 1995. Basin development and tectonic history of the Llanos Basin, Eastern Cordillera, and Middle Magdalena Valley, Colombia. American Association of Petroleum Geologists Bulletin, 79, 1421-1443.

Corredor, F., 2003a. Eastward extent of the Late Eocene–Early Oligocene onset of deformation across the northern Andes: constraints from the northern portion of the Eastern Cordillera fold belt, Colombia. Journal of South American Earth Sciences, 16, 445-457.

Corredor, F., 2003b. Seismic strain rates and distributed continental deformation in the northern Andes and three-dimensional seismotectonics of northwestern South America. Tectonophysics, 372, 147-166.

Cortes, M., Angelier, J., 2005. Current states of stress in the northern Andes as indicated by focal mechanisms of earthquakes. Tectonophysics, 403, 29-58.

Crespi, J.M., Chan, Y.C., Swaim, M., 1996. Synorogenic extension and exhumation of the Taiwan hinterland. Geology, 24, 247-250.

Dewey, J.F., 1988. Extensional collapse of orogens. Tectonics, 7, 1123-1139.

Duerto, L., Escalona, A., Mann, P., 2006. Deep structure of the Merida Andes and Sierra de Perija mountain fronts, Maracaibo Basin, Venezuela. AAPG Bulletin, 90, 505-528.

Ego, F., Sebrier, M., Lavenu, A., Yepes, H., Egues, A., 1996. Quaternary state of stress in the Northern Andes and the restraining bend model for the Ecuadorian Andes. Tectonophysics, 259, 101-116.

Freymueller, J.T., Kellogg, J.N., Vega, A.V., 1993. Plate motions in the Northern Andean region. Journal of Geophysical Research, 98, 21853-21863.

Giunta, G., Beccaluva, L., Siena, F., 2006. Caribbean Plate margin evolution: constraints and current problems. Geologica Acta, 4(1-2), 265-278.

Harris, L.B., Koyi, H.A., Fossen H., 2002. Mechanisms for folding of high-grade rocks in extensional tectonic settings. Earth-Science Reviews, 59, 163–210.

Hayashi, D., 2008. Theoretical basis of FE simulation software package. Bulletin of the Faculty of Science, University of the Ryukyus, 85(3), 81-95.

Hayashi, D., 1972. Numerical analysis of Migmatite dome with special reference to finite element method. Journal of the Geological Society of Japan, 78, 677-686.

Hodges, K.V., Parrish, R.R., Housh, T.B., Lux, D.R., Burchfiel, B.C., Royden, L.H., Chen, Z., 1992. Simultaneous Miocene extension and shortening in the Himalayan orogen. Science, 258, 1466-1470.

Introcaso, A., Pacino, M. C., Fraga, H., 1992. Gravity, isostasy and Andean crustal shortening between latitudes 30 and 35ºS. Tectonophysics, 205, 31-48.

Islam, M.R., Hayashi, D., 2008a. Numerical modeling of Neotectonic stress field and crustal deformation around basement faults of the Patagonian Orocline, Southernmost Andes. The 3rd COE-21 International Symposium, MISASA-III "Origin, Evolution and Dynamics of the Earth" in March 21-23, 2008, Okayama University, Japan. Abstract (volume), 165p.

Islam, M.R., Hayashi, D., 2008b. Extensional stresses in the fold-and-thrust belt of the Southernmost Andes. Bollettino di Geofisica Teorica ed Applicata, 49(2) Special Issue, 223-228.

Iturralde-Vinent, M.A., Lidiak, E.G., 2006a. Caribbean Plate Tectonics. Geologica Acta, 4, 1-341.

Iturralde-Vinent, M.A., Lidiak, E.G., 2006b. Caribbean Tectonic, Magmatic, Metamorphic and Stratigraphic Events. Implications for Plate Tectonics. Geologica Acta, 4, 1-5.

Jaillard, E., Solar, P., Carlier, G., Mourier, T., 1990. Geodynamic evolution of the northern and central Andes during early to middle Mesozoic times: a Tethyan model. Journal of Geological Society of London, 147, 1009-1022.

James, K.H., 2006. Arguments for and against the Pacific origin of the Caribbean Plate: discussion, finding for an inter-American origin. Geologica Acta, 4(1-2), 279-302.

Jolivet, L., Goffe, B., 2000. Extensional metamorphic domes in mountains belts, syn-orogenic and post-orogenic extension. Comptes Rendus de l'Academie des Sciences, Earth and Planetary Science Series IIA, 330, 739−751.

Klepeis K.A. and Austin J.J.A., 1997. Contrasting styles of superposed deformation in the southernmost Andes. Tectonics, 16, 755-776.

MacDonald, W.D., Estrada, J.J., Sierra, G.M.., Gonzalez, H., 1996. Late Cenozoic tectonics and paleomagnetism of North Cauca Basin intrusions, Colombian Andes: Dual rotation modes. Tectonophysics, 261, 277-289.

Malavielly, J., 1993. Late orogenic extension in mountain belts: insights from the basin and range and late Paleozoic Variscan belt. Tectonics, 12, 1115-1130.

Maze, W.B., 1984. Jurassic La Quinta Formation in the Sierra de Perija, northwestern Venezuela: geology and tectonic environment of red beds and volcanic rocks. In: Bonini, W.E., Hargraves, R.B., Sagam, R. (eds.). The Caribbean-South American plate boundary and regional tectonics. Geological Society of American Memoir, 162, 263-282.

McCourt, W.J., Aspden, J.A., Brook, M., 1984. New geological and geochronological data from the Colombian Andes: continental growth by multiple accretion. Journal of the Geological Society of London, 141, 831-845.

Megard, F., 1987. Cordillera Andes and marginal Andes: a review of Andean geology north of the Arica elbow (18 deg. S). In: Monger, J.W.H., Francheteau, J. (eds.). Circum-Pacific orogenic belts and evolution of the Pacific Ocean basin. American Geophysical Union, Geodynamic series, 18, 71-95.

Melosh, H.J., Williams, C.A., 1989. Mechanics of graben formation in crustal rocks: A Finite Element analysis. Journal of Geophysical Research, 94, 13961-13973.

Molina, A.C., Cordani, U.G., MacDonald, W.D., 2006. Tectonic correlations of pre-Mesozoic crust from the northern termination of the Colombian Andes, Caribbean region. Journal of South American Earth Sciences, 21, 337−354.

Molnar, P., Atwater, T., 1978. Interarc spreading and cordilleran tectonics as alternates related to the age of subducted oceanic lithosphere. Earth and Planetary Science Letters, 41, 330−340.

Montes, C.T., Hatcher, Jr., R.D., Restrepo, P.A., 2005. Tectonic reconstruction of the northern Andean blocks: Oblique convergence and rotations derived from the kinematics of the Piedras–Girardot area, Colombia. Tectonophysics, 399, 221-250.

Nivia, A., Marriner, G.F., Kerr, A.C., Tarney, J., 2006. The Quebradagrande Complex: A Lower Cretaceous ensialic marginal basin in the Central Cordillera of the Colombian Andes. Journal of South American Earth Sciences, 21, 423-436.

Pennington, W.D., 1981. Subduction of the Eastern Panama Basin and Seismotectonics of Northwestern South America Journal of Geophysical Research, 86, 10753-10770.

Pindell, J., Kennan, L., Draper, G., Maresch, W.V., Stanek, K.P., 2006. Foundations of Gulf of Mexico and Caribbean evolution: eight controversies resolved. Geologica Acta, 4(1-2), 303-341.

Richardson, R.M., Coblentz D.D., 1994. Stress modeling in the Andes: Constraints on the South American intraplate stress magnitudes. Journal of Geophysical Research, 99, 22015−22025.

Sarmiento, R.L.F, Van Wess, J.D., Cloetingh, S., 2006. Mesozoic transextensional basin history of the Eastern Cordillera, Colombian Andes: Inferences from tectonic models. Journal of South American Earth Sciences, 21, 383- 411.

Stephansson, O., Berner, H., 1971. The finite element method in tectonic processes. Physics of the Earth and Planetary Interior, 4, 301-321.

Suarez, A.F., 1990. The basement of the Eastern Cordillera, Colombia: an allochthonous terrane in the northwestern South America. Journal of South American Earth Sciences, 3, 141-151.

Suter, F., Neuwerth, R., Gorin, G., Guzman, C., 2008. (Plio) Pleistocene alluvial-lacustrine basin infill evolution in a strike-slip active zone (Northern Andes, Western-Central Cordilleras, Colombia). Geologica Acta, 6(3), 231-249.

Taboada, A., Rivera, L., Fuenzalida, A., Cisternas, A., Philip, H., Bijwaard, H., Olaya, J., Rivera, C., 2000. Geodynamics of the northern Andes: Subduction and intracontinental deformation (Colombia). Tectonics, 19, 787-813.

Timoshenko, S. P., Goodier, J.N., 1970. Theory of Elasticity. McGraw Hill Book Company, London, Third edition, 567pp, international edition, 488pp.

Trenkamp, R., Kellogg, J.N., Freymueller, J.T., Mora, H.P., 2002. Wide plate magin deformation, south Central America and northwestern South America, CASA GPS observations. Journal of South American Earth Sciences, 15, 157-171.

Vásquez, M., Altenberger, U., 2005. Mid-Cretaceous extension-related magmatism in the eastern Colombian Andes. Journal of South American Earth Sciences, 20, 193−210.

Willett, S.D., 1999. Rheological dependence of extension in wedge models of convergent orogens. Tectonophysics, 305, 419-435.

Zoback, M.L., 1992, First- and second-order patterns of stress in the lithosphere: The World Stress Map Project. Journal of Geophysical Research, 97, 11703−11728.

Manuscript received November 2007;
revision accepted June 2008;
published Online March 2009.